An Effective Discretization Method of Derivative Operator for the Active Damping Purpose in LCL-Filter Based Grid-Tied Inverters

H. Zamani[1,2]*, K. Abbaszadeh[1], M. Karimi[3], J. Gyselinck[2]

[1] Departments of Electrical Engineering, K. N. Toosi university of technology, Tehran, Iran (e-mail: H.zamani@email.kntu.ac.ir, abbaszadeh@kntu.ac.ir).

[2] Department of BEAM, Université Libre de Bruxelles (ULB), Belgium (e-mail: hasan.zamani@ulb.be, johan.gyselinck@ulb.be).

[3] Academic Center for Education Culture and Research, Tehran, Iran (e-mail: mhkarimi@jdnasir.ac.ir).

*Corresponding Author

Abstract—**For synchronization with the grid and controlling the injected active and reactive currents of the LCL-filter based grid-tied inverters, capacitor voltages can be sampled. An LCL filter attenuates the switching harmonics effectively but needs an extra sensor for the LCL filter resonance damping. Popular methods use capacitor currents for the LCL filter resonance damping. Theoretically, the derivative of capacitor voltage, which is proportional to the capacitor current, damps the resonance, and the extra sensor is avoided. However, traditional discretization methods for digital implementation of the derivative operator are not valid when the resonance frequency is high. Indeed, they don't preserve the phase and magnitude of the 's' function in the resonance frequency region. This paper introduces an effective method for discretizing the 's' function in the desired frequency range. The capacitor voltages of the LCL filter are sampled and the proposed function makes their derivative. The output of the derivative function with a tuned gain is added to the controller's output for damping the LCL filter resonance. The simulation results show the effectiveness of the proposed method.**

*Keywords***: LCL filter, Grid-tied inverter, resonance damping, discretization method.**

I. INTRODUCTION

Grid-tied inverters as the interface between the grid and renewable-energy systems have received increasing attention recently. To inject current with low Total Harmonic Distortions (THD) and meet the grid standards, an L or LCL filter is usually integrated between the inverter and power grids. The LCL filter attenuates the switching harmonics more effectively, but introduces two poles on the imaginary axis whose frequency is called the LCL filter resonance and makes the closed-loop system unstable [1]-[6].

The LCL resonance damping methods are mainly divided into passive damping (PD) and Active Damping (AD). PD adds a resistor in parallel or series with elements of the LCL filter, which increases losses and thus decreases the total efficiency. Therefore, this approach is unsuitable for high current applications. AD uses the PD resistor effect in the closed-loop system by manipulating the Mason graph of the system and needs an extra sensor.

AD can be achieved by measuring different state variables of the LCL filter. It can be based on the inverter-side currents [7], [8], the capacitor currents [9], [10], the capacitor voltages [11]-[14], and the grid-side currents [6], [15]. Theoretically, it is possible to reduce the proportional gain of the closed-loop regulators to stabilize the system. However, this technique has serious disadvantages such as low controller bandwidth and poor disturbance rejection.

Modern control approaches such as Sliding Mode Control (SMC), Deadbeat Predictive Control (DPC), and state feedback control have been proposed in [6]-[20]. Basically, using these controllers does not eliminate the need for extra sensors for resonance damping. In [21], an adaptive sliding mode controller is designed to regulate the grid-side currents. The resonance frequency of the implemented LCL filter is above one-sixth (critical frequency) of the sampling frequency. It is proved in [22] that LCL filters whose resonance frequency is above the critical frequency do not need AD. However, setting the LCL resonance frequency above the critical frequency

does not allow using all abilities of the LCL filter in attenuation of switching harmonics.

Considering the inverter-side currents as the control targets provides stability against the LCL filter resonance [23]. But, this approach does not have enough precision in the control of both the power factor and the waveform of the injected current into the grid [18], [24]. In [25], the proposed control algorithm has six loops for regulating the inverter-side current, the grid-side currents, and the capacitor voltages. Also, four estimators for reducing sensors are used. Even though the control approach fulfills the requirements, it needs a complex tuning procedure.

AD with adding a resistor effect in the control loop is a partial state feedback, which moves the unstable poles of the LCL filter inside the stability region. The closed-loop poles are assigned in arbitrary locations by the full state feedback and generate the desired dynamic response. However, this method needs as many sensors as the system states [26]. Some attempts have been made to reduce additional sensors by using observers [27], [28]. However, the estimation adds computational cost to the control system.

For synchronization with the grid and injecting current with controlled phase and amplitude, the grid voltages or LCL capacitor voltages are sampled. Adding the derivative of the capacitor voltages to the controller's output with a tuned gain damps the LCL resonance. Thus, the need for the capacitor current sensors for AD can be removed. This is more interesting in high current applications where the current sensors are expensive. The problem comes from discretizing the derivative function ('s') when the resonance frequency is high. A discretization method has to preserve the magnitude and the phase of the ideal 's' function at the LCL resonance frequency. Traditional methods such as forward Euler, backward Euler, or Tustin do not fulfill the requirements [34]. The backward Euler does not preserve the phase of the ideal 's' function. The forward Euler always adds unstable poles to the system and it is not recommended. The Tustin method amplifies noise, and this method is not valid at the LCL resonance frequency.

Different approaches are suggested for the digital implementation of the 's' function [11]-[13], [29]. In [11], a high pass filter makes the derivative of the capacitor voltages. The high pass filter is tuned to preserve features of the 's' function at the resonance frequency. A high pass filter mimics the 's' function below a specific cutoff frequency. For higher frequencies, it generates phase error in the response.

In [29], capacitor voltages are passed through a low pass filter and the outputs are used for AD. In the steady-state condition, a low pass filter is an integrator whose output is delayed by $90°$. The negative of this filter is advanced by $90°$ and mimics the derivative function. However, this method is not valid during the transient state, and

therefore this method is not a true derivative. In [12] and [13], a lead-lag filter makes the derivative of capacitor voltages. This filter is valid in a narrow frequency range, and has a complex tuning procedure. This problem is more significant when the inverter is connected to a weak grid where the resonance frequency changes frequently [33].

It is worth noting that every techniques for the discretization of the 's' function must not amplify noise at high frequencies.

This paper introduces a method for constructing a discrete function that preserves the 's' function in a desire frequency range. The phase and magnitude of the proposed function and the ideal 's' function are matched in the selected frequency range which includes the resonance frequency.

The rest of the paper is organized as follows. In section II, the dynamic model of the process is derived in the stationary frame. In this section, a brief discussion about the LCL filter resonance is given. In section III, the linear system identification method for construction of a discrete function that mimics the 's' function is explained. A comprative study is given to show the superiority of the proposed function over the other methods. In section IV, the AD gain based on the root loci analysis is tuned. To verify the effectiveness of the proposed function, simulation results are given in V. Finally, the conclusion is given in VI.

II. SYSTEM MODELING

Fig.1 shows a 3-phase grid-tied inverter. To inject current with low THD, an LCL filter is integrated between the inverter and the grid. Table I shows the parameters under study. The dynamic system equation according to Fig.1 in the stationary reference frame is:

$$v_{abc}^i = r_L i_{abc}^i + l_1 \frac{di_{abc}^i}{dt} + v_{abc}^1 \qquad (1)$$

$$v_{abc}^1 = r_L i_{abc}^g + l_2 \frac{di_{abc}^g}{dt} + v_{abc}^g \qquad (2)$$

$$v_{abc}^1 = v_{abc}^c + r_c i_{abc}^c \qquad (3)$$

$$i_{abc}^i = i_{abc}^c + i_{abc}^g . \qquad (4)$$

i and g superscripts denote the inverter-side and the grid-side variables. v_{abc}^1 is the voltage drop across the capacitor filter and its parasitic resistance. In the worst case, where the parasitic resistances are neglected, and the resonance is strong, the transfer function between one phase of the grid current and the inverter voltage is expressed as follows:

$$Gc_{undamped} = \frac{i^g}{v^i} = \frac{1}{l_1 s} \frac{\gamma^2}{s^2 + \omega_{res}^2} \qquad (5)$$

where:

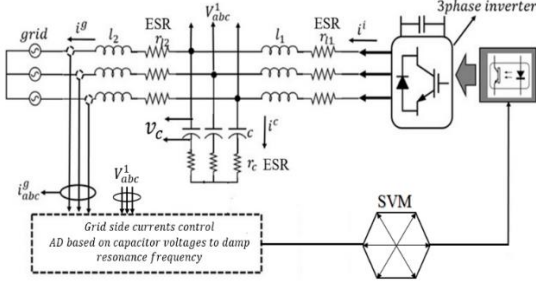$$\omega_{res} = \sqrt{\frac{l_1 + l_2}{l_1 l_2 c}} , \gamma = \frac{1}{\sqrt{l_2 c}}.$$

Fig. 1. Configuration of a 3-phase grid-tied inverter.

Fig. 2: Grid-side current control with two possibilities for AD.

As (5) shows, there are two poles on the imaginary axis that can make the closed-loop system unstable. Fig. 2 shows control schemes when the grid-side currents are the control targets. In this figure, two strategies for AD are shown. In the first strategy, the capacitor current with a tuned gain (G_{AD}) is added to the controller's output ($v_{control}$). This modification in the control loop damps the LCL filter resonance. To show this, (5) can be written as:

$$\frac{i^g}{v^i} = \frac{i^g}{v_{control} - G_{AD}i^c} = \frac{1}{l_1 l_2 cs} \frac{1}{s^2 + \omega_{res}^2} \quad . \tag{6}$$

By using $i^c = csv^c$ in (2) and setting r_l and v_{abc}^g to zero, the relation between i^c and i^g is obtained:

$$v^1 = v^c = \frac{1}{cs} i^c l_2 s i^g$$

Considering the second term and the third term in the above equation results in:

$$i^c = cl_2 s^2 i^g. \tag{7}$$

A cross-multiplying of the second and third terms of (6) and using i^c from (7) results in:

$$i^g\left(l_1 l_2 cs(s^2 + \omega_{res}^2)\right) = v_{control} - G_{AD}cl_2 s^2 i^g.$$

Finally, the transfer function relating i^g and $v_{control}$ is:

$$Gc_{damped} = \frac{i^g}{v_{control}} = \frac{1}{l_1 l_2 cs} \frac{1}{s^2 + K_d s + \omega_{res}^2} \tag{8}$$

where

$$K_d = \frac{G_{AD}}{l_1}.$$

Gc_{damped} has a standard form of the well-known second-order transfer function. In this transfer function, K_d is the damping ratio. Comparing (5) and (8) shows that adding the capacitor current to the controller's output shifts the unstable poles toward the left-hand side of the s-plane.

Fig. 3 shows the Bode diagrams of $Gc_{undamped}$ and Gc_{damped}. The former shows an infinite gain around the resonance frequency while a sharp crossing of -180 degrees occurs in the phase diagram. This means instability in the closed-loop system [30]. This infinite gain doesn't exist in the Bode diagram of Gc_{damped}.

To synchronize with the grid and inject currents with a controlled phase and amplitude, the capacitor voltages can be sampled. In the continuous space, the derivative of the capacitor voltage is proportional to the capacitor current and can be used for AD. However, traditional discretization methods are not valid around the resonance frequency. In the next section, a systematic procedure for constructing a discrete function that preserves the 's' function in a desire frequency range is explained. The transfer function is in the 'z' domain and is valid at the resonance frequency.

III. LINEAR SYSTEM IDENTIFICATION

A. Extraction of a discrete derivative transfer function for digital implementation

Methods in the system identification theory try to construct a dynamic model based on the measured data. An identification needs three steps: data collection,

TABLE I
PARAMETERS UNDER THE STUDY

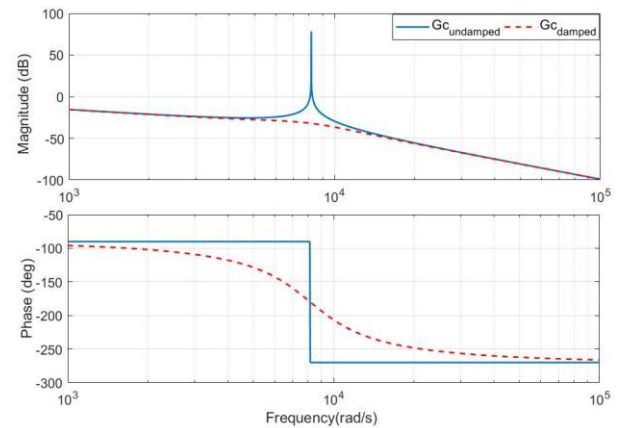| Symbol	quantity	Value
l_1	Inverter-side filter inductance	3 mH
l_2	Grid-side inductance	1.2 mH
c	Filter Capacitor	10 μF
V_{dc}	DC bus voltage	650V
v^g	Grid voltage	380V rms
f_{sw}	Switching frequency	10 kHz
f_{res}	Resonance frequency	1.7 kHz
f	Grid frequency	50 Hz

Fig. 3. Bode diagrams of Gc_{damped} (red curve) and $Gc_{undamped}$ (blue curve).

model selection, and model validation [31]. In one view, linear identification methods can be classified into time-domain and frequency-domain methods. In this research, a time-domain method for constructing the derivative function is developed. The most important time-domain models are Autoregressive with Exogenous Input (ARX), Autoregressive Moving Average with Exogenous Input (ARMAX), Output Error (OE), and Box-Jenkins (BJ) [۳۱]. Selection of a model usually starts with the simplest available ones. Therefore, ARX is the first approach for modeling the derivative function. The structure of 1-input, 1-output ARX is:

$$A(z^{-1})y = B(z^{-1})u + e \qquad (9)$$

with A and B the polynomials, u and y the input and output of the model and e the white noise with zero average. A and B polynomials have the following forms:

$$A(z^{-1}) = 1 + a_1 z^{-1} + \cdots + a_{na}z^{-n_a} \qquad (10)$$

$$B(z^{-1}) = b_0 z^{-1} + \cdots + b_{nb}z^{-n_b}. \qquad (11)$$

To obtain the ARX parameters, the system (the 's' function) must be persistently excited.

Variations in the grid inductance result in deviations in the LCL filter resonance frequency. The derivative function should be valid in a reasonable frequency range that covers resonance frequency changes. The frequency range between 1.3 kHz and 1.7 kHz is selected for constructing the desired function. A mixture of sinusoidal signals that cover this frequency range is used for the excitation signal. It is possible to extend the valid frequency range, but the order of the transfer function increases, also. Fig. 4 shows the excitation scheme which is done in MATLAB Simulink. The 's' function is fed with a chirp signal. The data of the chirp signal and the 's' function output is recorded for the identification. The sampling frequency is 10 kHz. The goal is to find the model output $\hat{y}$ that best approximates the sampled output y by optimizing the ARX parameters (the A and B polynomials). (9) can be rewritten in the following form:

$$\hat{y} = \varphi_t \theta^T + e \qquad (11)$$

with θ^T the ARX parameters, $\hat{y}$ the estimated output and φ_t the regressors:
$$\theta = [a_1, \ldots, a_{na}, b_0, \ldots, b_{nb}]$$

$$\varphi_t = [-y(t-1), \ldots, -y(t-n_a), u_1(t-1), \ldots, u_1(t-n_b)].$$

θ^T is obtained by minimizing the sum squared errors between y and $\hat{y}$:
$$J(\theta) = \sum_{t=1}^{N}\big(y(t) - \hat{y}(t)\big)^2 = \sum_{t=1}^{N}\big(y(t) - \varphi_t\theta^T\big)^2 \qquad (12)$$

with N the number of the sampled data. By setting the derivative of J with respect to θ^T to zero, the ARX parameters are obtained:

$$\theta^T = \left[\frac{1}{N}\sum_{t=1}^{N}\varphi_t^T\varphi_t\right]^{-1}\left[\frac{1}{N}\sum_{t=1}^{N}\varphi_t^T y(t)\right] \qquad (13)$$

More detail is explained in [31].

Selection of ARX polynomial orders (n_a, n_b) is a challenging procedure, which in most cases is based on trial and error. To determine the lowest orders for the best fit, different values of n_a and n_b were examined. The best fit with sufficient accuracy is achieved with $n_a = 2$ and $n_b = 2$ which is 99 %. The obtained transfer function is:

$$D = \frac{1.739 \times 10^4 z^2 - 1.786 \times 10^4 z}{z^2 + 8.682 \times 10^{-1}z + 0.044 \times 10^{-5}}. \qquad (14)$$

B. Validation of the derivative transfer function and a comparative study

Table II shows the backward-Euler, forward-Euler, and Tustin methods for discretization. The Bode diagrams of these three functions and the 's' function for the frequencies between 1.3 kHz and 1.7 kHz are shown in Fig. 5.

The Bode diagram shows that the phase and magnitude of forward and backward Euler derivatives diverge from the 's' function, which are not acceptable. The Bode diagram of Tustin is matched with the 's' function. But this method amplifies the sampling noise. For more investigation, the time domain responses of the Tustin function and the 's' function are shown in Fig . 6. The frequency of the input signal is f = 1.4 kHz. As can be seen, the obtained waveforms by Tustin and the continuous 's' function are not matched, and the Tustin method is not acceptable for this application.

Also, the time domain responses of the backward Euler function and the 's' function are shown in Fig. 7. The frequency of the input signal is 1.4 kHz. The phase error between the 's' function and backward Euler function is observed.

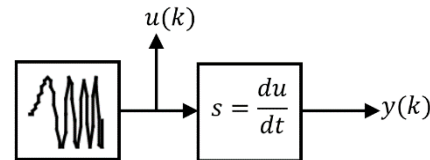The Bode diagrams of the D function and the 's' function

Fig. 4. Excitation signal.

TABLE II
DIRECT DISCRETIZATION METHODS

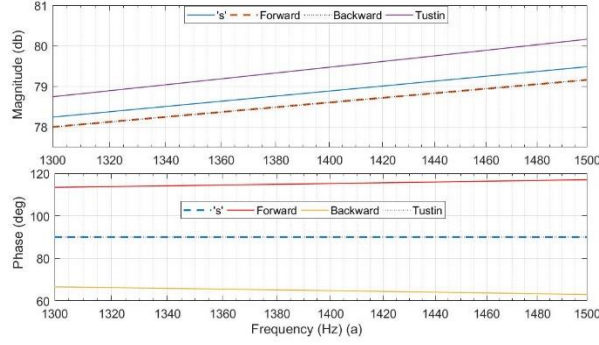| Method	Transfer function
Tustin	$\frac{2}{T_s}\frac{z-1}{z+1}$
Forward-Euler	$\frac{z-1}{T_s}$
Backward-Euler	$\frac{z-1}{zT_s}$

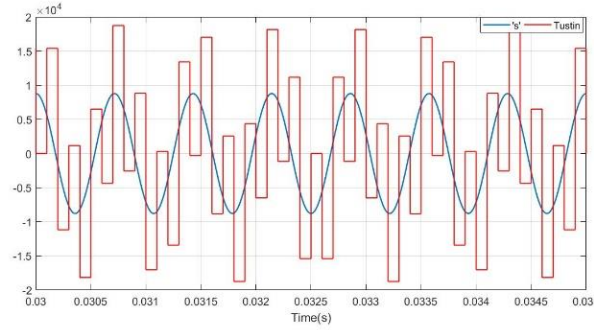Fig. 5. Bode diagrams of Tustin, backward-Euler, and forward-Euler derivatives.

Fig. 6. The outputs of the 's' function and the Tustin function, the frequency of the input signal is 1.4 kHz .

are shown in Fig. 8. The D function shows $90°$ phase at the resonance frequency which is in agreement with the 's' function. The output waveforms of the D and 's' functions are demonstrated in Fig. 9. The frequency of the input signal is f=1.5 kHz. The obtained results show a good match between the magnitude and the phase of D and 's' functions.

Furthermore, the D function is valid with less than a $0.5°$ error in the phase in the frequency range of [1.3 1.7] kHz. The D function makes the capacitor voltage derivative, and the capacitor current information around the resonance frequency is preserved.

For more investigation, the Bode diagram of a lead-lag filter, which is presented in [12], is shown in Fig. 10. The transfer function of the lead-lag filter is:

$$H = k_d C \; \omega_{max} \left(\frac{s + k_f \omega_{max}}{k_f s + \omega_{max}} \right) \tag{15}$$

with k_f the following coefficient:

$$k_f = \sqrt{\frac{1 - \sin \varphi_{max}}{1 + \sin \varphi_{max}}}$$

and with ω_{max} the frequency for the maximum phase (which is set at the resonance frequency), φ_{max} the

maximum phase at ω_{max}, k_d the damping factor. Following the procedure, which is explained in [12], the filter is designed for an LCL filter whose resonance frequency is 1.5 kHz. The phase error of this filter at resonance frequency is about $13°$.

IV. AD AND PI CONTROLLER DESIGN

To tune the coefficients of the Proportional-Integrator (PI) controller for tracking the grid-side current, the LCL filter below the resonance frequency is approximated with an
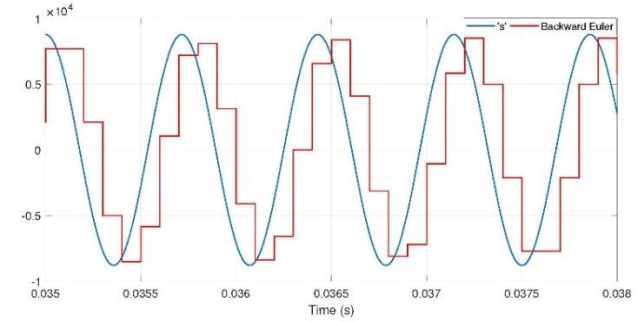

Fig. 7. The outputs of the backward Euler and 's' functions, the input signal frequency is 1.5 kHz.
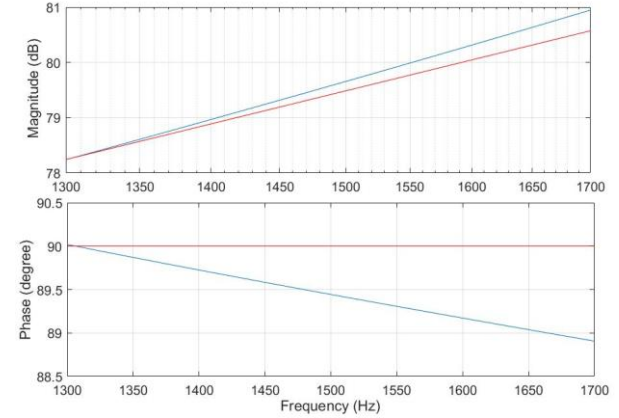

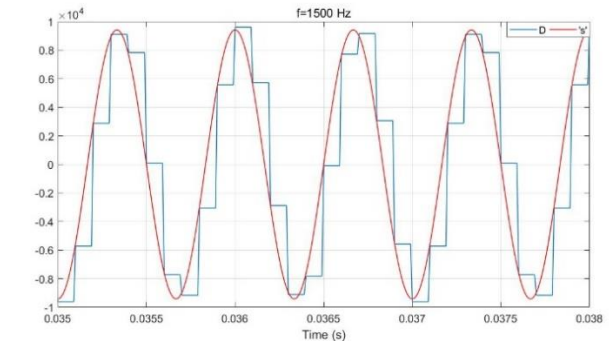Fig. 8. Bode diagrams of D and 's' transfer functions.

Fig. 9. The outputs of the D and 's' functions, the input signal frequency is 1.5 kHz.
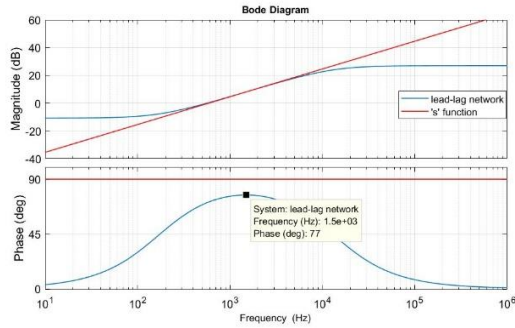
Fig. 10. Bode diagrams of the lead-lag network and the 's' function.

inductance. The value of this inductance is the sum of the grid-side and the inverter-side inductances. With this simplification, coefficients of the PI controller can be tuned with the symmetrical optimum design [32]:

$$K_p = \frac{l_1 + l_2}{3T_s} \qquad (16)$$

$$T_i = 9T_s$$
$$K_i = \frac{K_p}{T_i}$$

with K_p the proportional gain, K_i the integral gain, and T_i the integrator time constant.

The AD gain (G_{AD}) is tuned by the root-locus method. First, the closed-loop transfer function is derived. Then, the dominator of the transfer function whose zeros determine the closed-loop poles is modified such that G_{AD} appears as a multiplying factor. The open-loop transfer function according to Fig. 2 is:

$$G = PI \times G_{vcontrol}^{ig} . \qquad (17)$$

$G_{vcontrol}^{ig} = \frac{i^g}{v_{control}}$ is the transfer function relating the PI controller output ($v_{control}$) and the grid-side current. This function can be written in two terms:

$$G_{vcontrol}^{ig} = G_{control}^{vc} \times G_{vc}^{ig} . \qquad (18)$$

Where $G_{vc}^{ig} = \frac{i^g}{v_c}$, and $G_{control}^{vc} = \frac{v^c}{v_{control}}$. G_{vc}^{ig} is the transfer function relating the capacitor voltage and the grid-side current:

$$G_{vc}^{ig} = \frac{1}{l_2 s}. \qquad (19)$$

Using (18) in (17) results in:

$$G = PI \times G_{control}^{vc} \times G_{vc}^{ig}. \qquad (20)$$

$G_{control}^{vc}$ is the transfer function relating the capacitor

voltage and $v_{control}$. This function is obtained by considering the relationship between the capacitor voltage and the inverter voltage which is:

$$G_{vi}^{vc} = \frac{v^c}{v^i} = \frac{1}{l_1 cs + \frac{l_1 + l_2}{l_2}} . \qquad (21)$$

(21) is obtained from (1)-(5). According to the control scheme presented in Fig. 2, v^i is $v^i = v_{control} - G_{AD}cDv^c$. Using the equivalent expression of v^i in (21) yields:

$$G_{vi}^{vc} = \frac{v^c}{v^i = v_{control} - G_{AD}cDv^c} = \frac{1}{l_1 cs + \frac{l_1 + l_2}{l_2}} \qquad (22)$$

A cross-multiplying between the first term and second term of (22) results in:

$$G_{vi}^{vc}(v_{control} - G_{AD}cDv^c) = v^c$$

and finally $G_{control}^{vc}$ is:

$$G_{control}^{vc} = \frac{v^c}{v_{control}} = \frac{G_{vi}^{vc}}{1 + G_{vi}^{vc} G_{AD}cD} \qquad (23)$$

All the transfer functions in (20) have been determined and the closed-loop transfer function can be obtained as:

$$T = \frac{G}{1 + G} . \qquad (24)$$

By setting $(1 + G)$ to zero (the characteristic equation of T), the closed-loop poles are obtained:

$$1 + G = \frac{1 + G_{vi}^{vc} G_{AD}cD + PI\ G_{vi}^{vc} G_{vc}^{ig}}{1 + G_{vi}^{vc} G_{AD}c\ D} = 0 \qquad (25)$$

which results in:

$$1 + G_{vi}^{vc} G_{AD}c\ D + PI\ G_{vi}^{vc} G_{vc}^{ig} = 0. \qquad (26)$$

(26) is modified such that G_{AD} appears as a multiplying factor:

$$1 + \frac{G_{AD} G_{vi}^{vc} cD}{1 + PI\ G_{vi}^{vc} G_{vc}^{ig}} = 0. \qquad (27)$$

Fig. 11 shows the loci of the closed-loop poles as G_{AD} is varied. The value of G_{AD} which provides the highest stability is 23 Ω.

For more investigation, the step response of the T transfer function with the tuned coefficients of the PI controller and the AD gain is given in Fig. 12. The settling time is 2 ms, and the overshoot is negligible. This figure shows that there is no oscillation in the response, and the LCL resonance is damped.

The robustness of the closed-loop system against the model mismatches is measured by the phase margin. The phase margin is the distance to the -180° phase value in the Bode diagram at the cut-off frequency. The Gain Margin (GM) and Phase Margin (PM) of the open-loop transfer function (G in (17)) are obtained by MATLAB and are 7.54 dB and 57.5° which fulfil the requirements of a stable system (Fig. 13).

Fig. 14 demonstrates the Bode diagram of the damped system with the proposed AD. Also, the undamped system is shown. The former shows no infinite gain,

6

which confirms the stability of the closed-loop system. Table III shows PM and GM for three different values of grid-side inductances. This table shows that the system has enough robustness against the grid-side inductance variations.
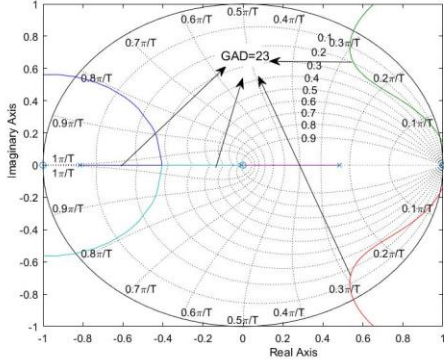

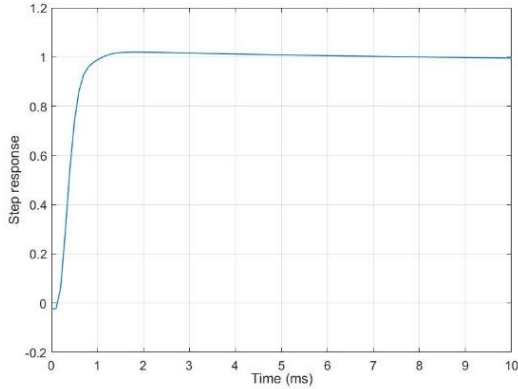Fig. 11. Closed-loop poles displacement by G_{AD} variations.

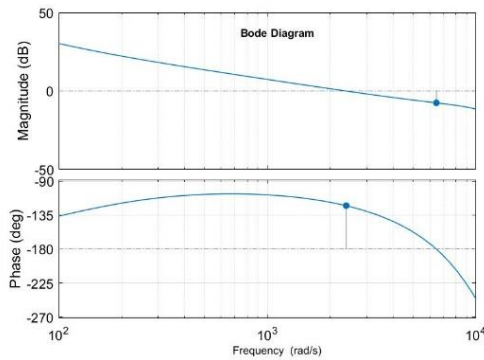Fig. 12. Step response of the T transfer function, $G_{AD} = 23$.

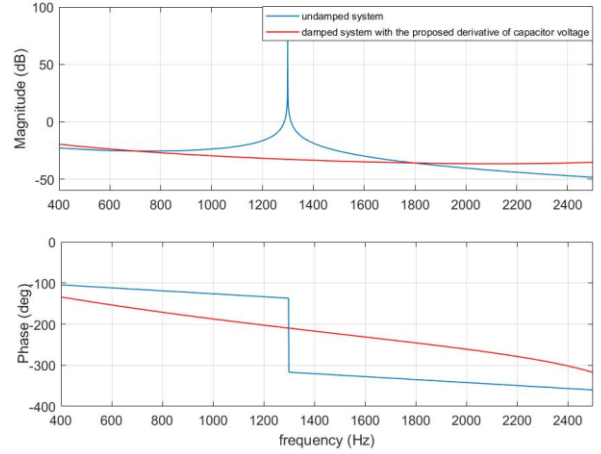Fig. 13. GM and PM with AD based on the capacitor voltage differentiated by the D function.

Fig. 14. The Bode diagrams of damped system with the proposed derivative method and undmaped system, $G_{AD} = 23$.

TABLE III
A SUMMARY OF PM AND GM FOR DIFFERENT VALUES OF THE GRID INDUCTANCE (THE D FUNCTION MAKES DERIVATIVE OF THE CAPACITOR VOLTAGE FOR AD).

Value of inductance (l_2)	GM (dB)	PM (degree)
$3\ mH\ (f_{res} = 1.3\ kHz)$	7.45	59
$2.5\ mH\ (f_{res} = 1.37\ kHz)$	7.23	58
$1.2\ mH\ (f_{res} = 1.7\ kHz)$	6.87	57.5

V. SIMULATION RESULTS

The entire system, including the inverter, SVM, and the controller, is simulated in MATLAB/Simulink for performance validation. The simulation parameter values are listed in Table I. The capacitor's voltages are sampled every 10 kHz for synchronization and AD purposes. The AD gain is tuned by the root-locus method ($G_{AD} = 23.0$). The control block diagram is shown in Fig. 15.

Fig. 16 shows the transient response of the closed-loop system. The grid-side currents in the synchronous and stationary reference frames are shown. In addition, the inverter-side currents in the stationary frame are demonstrated.
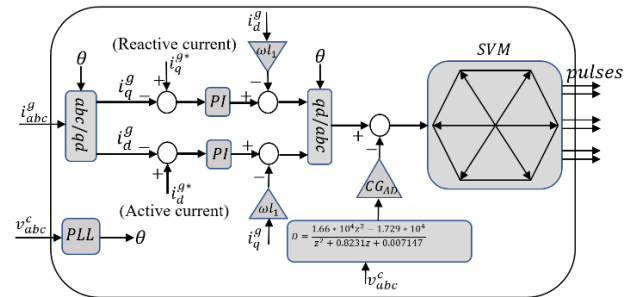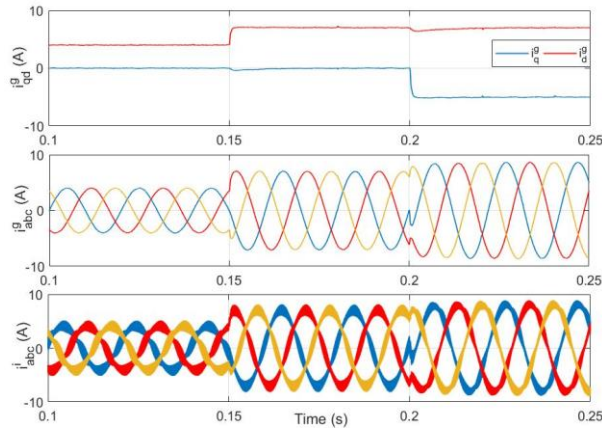

Fig. 15. The Overall control unit.

Fig. 16. Grid-side currents in the synchronous and stationary reference frames and inverter currents, d axis is stepped up: 4 A to 7 A at t=0.15 s, q axis is stepped down: 0 A to -5 A at t=0.2 s.

In this test, the d-axis reference current is stepped up from 4 A to 7 A at t = 0.15 s, and the q-axis reference current is stepped down from 0 to -5 A at t = 0.2 s. The settling time is less than 3 ms, and there is no overshoot in the response. No resonance is observed neither in the transient nor in the steady-state responses of both the q and d axes, which means the LCL filter resonance is damped.

By comparing the inverter-side currents and the grid-side currents, the effectiveness of the LCL filter is observed as the switching harmonics are eliminated in the grid-side currents.

The capacitor currents, capacitor voltages, and currents that are generated by differentiated capacitor voltages (iD_{abc}) with the D function are shown in Fig. 17. Some harmonics in iD_{abc} are filtered, but it still includes information which is necessary for the LCL filter
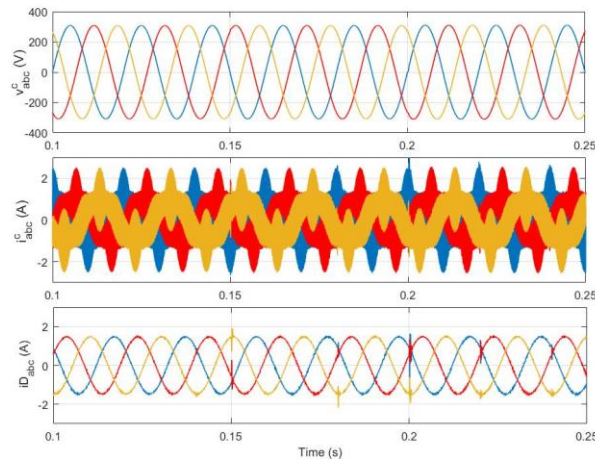

Fig. 17. The capacitor currents, capacitor voltages, and currents that are generated by the D function (iD_{abc})

resonance damping.

In the next test, the derivative method changes from the D function to the backward Euler function. This change occurs at t=0.08 s. For this transition, the AD gain and PI controller parameters remain unchanged. Therefore, the changes in system responses are solely triggered by the changes in the derivatives.

Fig. 18 shows the results. By applying the backward Euler derivative, the controller response starts oscillating, and the system becomes unstable.

The impedance of a weak grid changes frequently. As the impedance of the grid is in series with l_2, uncertainty in l_2 reflects the grid impedance variations [13]. In a test, the grid-side inductance (l_2) is stepped up at t =0.1 ms from 1.2 mH to 3 mH and is backed at t = 0.16 ms. Fig. 19 shows the results. This simulation shows that the disturbance is rejected successfully in less than 2 ms, and the system has an acceptable bandwidth. In addition, no oscillation is observed in the transient response, which
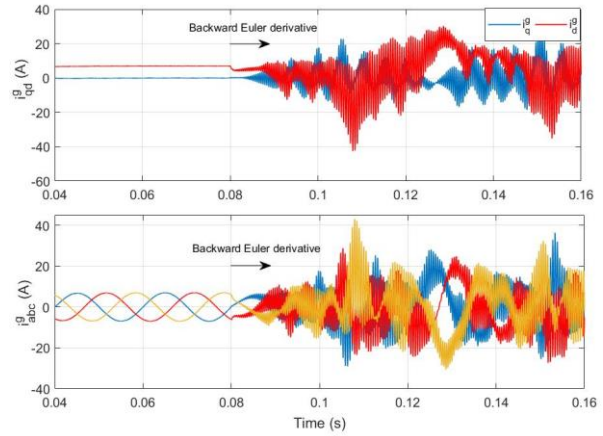

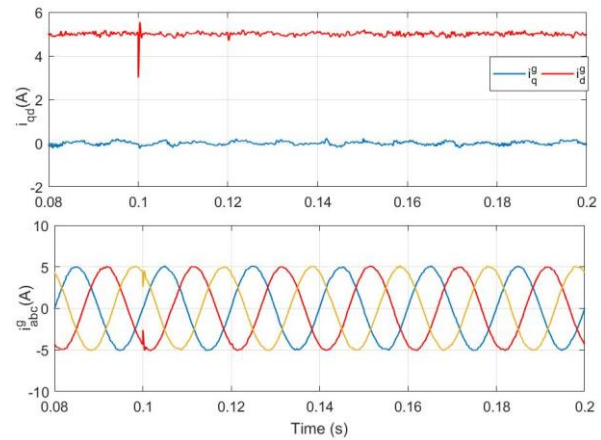Fig. 18. Derivation changes between the proposed method and backward Euler method at t=0.08s.

Fig. 19. l_2 step up: 1.2 mH to 3 mH (t = 0.04s), l_2 step dwon: 3mH to 1.2mH (t = 0.06ms).

8

confirms the effectiveness of the proposed derivative function.

In the next simulation, the performance of the closed-loop system is evaluated in terms of a grid voltage dip. A voltage dip is a disturbance where the RMS value of the line voltage is reduced by less than 500 ms. A grid voltage dip of 10 % is applied at t=0.08 s. The controller has coped with this disturbance in less than 12 ms (Fig. 20), and the currents follow their references accurately. Again, there are no oscillations in the transient response.

VI.   Conclusion

To control the injected active and reactive currents of the LCL-filter based grid-tied inverters, capacitor voltages can be sampled for synchronization with the grid. Theoretically, the derivative of capacitor voltages can be used to damp the LCL filter resonance, and extra sensors are avoided. However, when the resonance frequency is high, discretization methods for digital implementation of the derivative are not valid. Indeed, the phase and magnitude of the 's' function are not preserved in the resonance frequency region and AD based on derivative of the capacitor voltage is not effective. This paper introduced a method for constructing a discrete function that preserves the 's' function features in the desire frequency range. The selected frequency range was [1.3 1.7] kHz which includes the LCL filter resonance frequency. The orders of numerator and denominator of the obtained transfer function are 2. The larger frequency range, the higher order function is needed. The phase error between the proposed derivative function and the 's' function in the selected frequency range is less than $0.5°$. The phase error between the forward Euler and the 's' function is $30°$, and between the backward Euler and the 's' function is $-30°$ which are not acceptable. The phase of Tustin method is matched but it was shown that
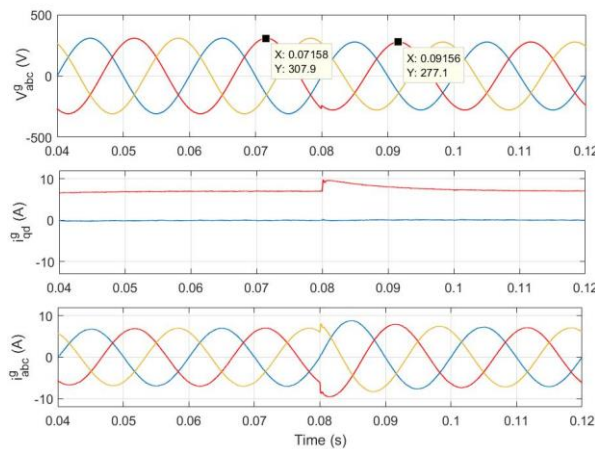

Fig. 20. Performance of the PI controller with the proposed derivative function for AD under a 3-phase grid voltage dip of 10 %.

this method amplifies noise and is not suitable for this application.

The AD gain (G_{AD}) was tuned by the root-locus method. The obtained phase margins for different non-nominal grid inductances were more than $57°$, which implies a robust closed-loop system. In the end, the results verified the effectiveness of the proposed method.

REFERENCES

[1] D. Pan, X. Ruan, C. Bao, W. Li, and X. Wang, "Capacitor-current-feedback active damping with reduced computation delay for improving robustness of lcl-type grid-connected inverter," *IEEE Transactions on Power Electronics*, vol. 29, no. 7, pp. 3414–3427, 2013.

[2] J. He and Y. W. Li, "Generalized closed-loop control schemes with embedded virtual impedances for voltage source converters with lc or lcl filters," *IEEE Transactions on Power Electronics*, vol. 27, no. 4, pp. 1850–1861, 2011.

[3] C. Bao, X. Ruan, X. Wang, W. Li, D. Pan, and K. Weng, "Step-by-step controller design for LCL-type grid-connected inverter with capacitor–current feedback active-damping," *IEEE Transactions on Power Electronics*, vol. 29, no. 3, pp. 1239–1253, 2013.

[4] V. Miskovic, V. Blasko, T. M. Jahns, A. H. Smith, and C. Romenesko, "Observer-based active damping of LCL resonance in grid-connected voltage source converters," *IEEE Transactions on Industry Applications*, vol. 50, no. 6, pp. 3977–3985, 2014.

[5] X. Wang, F. Blaabjerg, and P. C. Loh, "Design-oriented analysis of resonance damping and harmonic compensation for LCL-filtered voltage source converters," *in 2014 International Power Electronics Conference* (IPEC-Hiroshima 2014-ECCE ASIA), pp. 216–223. IEEE, 2014.

[6] X. Wang, F. Blaabjerg, and P. C. Loh, "Grid-current-feedback active damping for LCL resonance in grid-connected voltage-source converters," *IEEE Transactions on Power Electronics*, vol. 31, no. 1, pp. 213–223, 2015.

[7] A. J. Xu, B. S. Xie, C. J. Kan, and D. L. Ji, "An improved inverter-side current feedback control for grid-connected inverters with LCL filters," *in 2015 9th International Conference on Power Electronics and ECCE Asia* (ICPEECCE Asia), pp. 984–989. IEEE, 2015.

[8] L. Zhou, X. Zhou, Y. Chen, Z. Lv, Z. He, W. Wu, L. Yang, K. Yan, A. Luo, and J. M. Guerrero, "Inverter-current-feedback resonance-suppression method for LCL-type dg system to reduce resonance-frequency offset and grid-inductance effect," *IEEE Transactions on Industrial Electronics,* vol. 65, no. 9, pp. 7036–7048, 2018.

[9] D. Pan, X. Ruan, C. Bao, W. Li, and X. Wang, "Capacitor-current-feedback active damping with

reduced computation delay for improving robustness of LCL-type grid-connected inverter," *IEEE Transactions on Power Electronics*, vol. 29, no. 7, pp. 3414–3427, 2013.

[10] X. Li, X. Wu, Y. Geng, X. Yuan, C. Xia, and X. Zhang, "Wide damping region for LCL-type grid-connected inverter with an improved capacitor current-feedback method," *IEEE Transactions on Power Electronics*, vol. 30, no. 9, pp. 5247–5259, 2014.

[11] Malinowski, Mariusz, and Steffen Bernet. "A simple voltage sensorless active damping scheme for three-phase PWM converters with an $ LCL $ filter." *IEEE Transactions on Industrial Electronics* 55.4 (2008): 1876-1880.

[12] R. Pe˜na-Alzola, M. Liserre, F. Blaabjerg, R. Sebasti´an, J. Dannehl, and F. W. Fuchs, "Systematic design of the lead-lag network method for active damping in LCL-filter based three phase converters," *IEEE Transactions on Industrial Informatics*, vol. 10, no. 1, pp. 43–52, 2013.

[13] V. Blasko and V. Kaura, "A novel control to actively damp resonance in input LC filter of a three-phase voltage source converter," *IEEE Transactions on Industry Applications*, vol. 33, no. 2, pp. 542–550, 1997.

[14] V. Blasko and V. Kaura, "A novel control to actively damp resonance in input LC filter of a three-phase voltage source converter," *IEEE Transactions on Industry Applications*, vol. 33, no. 2, pp. 542–550, 1997.

[15] J. Xu, S. Xie, and T. Tang, "Active damping-based control for grid-connected LCL-filtered inverter with injected grid current feedback only," *IEEE Transactions on Industrial Electronics*, vol. 61, no. 9, pp. 4746–4758, 2013.

[16] R. Guzman, L. G. de Vicu˜na, M. Castilla, J. Miret, and H. Martin, "Variable structure control in natural frame for three-phase grid-connected inverters with LCL filter," *IEEE Transactions on Power Electronics*, vol. 33, no. 5, pp. 4512–4522, 2017.

[17] W. Jiang, W. Ma, J. Wang, L. Wang, and Y. Gao, "Deadbeat control based on current predictive calibration for grid-connected converter under unbalanced grid voltage," *IEEE Transactions on Industrial Electronics*, vol. 64, no. 7, pp. 5479–5491, 2017.

[18] C. A. Busada, S. G. Jorge, and J. A. Solsona, "Full-state feedback equivalent controller for active damping in LCL-filtered grid-connected inverters using a reduced number of sensors," *IEEE Transactions on Industrial Electronics*, vol. 62, no. 10, pp. 5993–6002, 2015.

[19] P. Karamanakos, R. Mattila, and T. Geyer, "Fixed switching frequency direct model predictive control based on output current gradients," *in IECON 2018 - 44th Annual Conference of the IEEE Industrial Electronics Society*, pp. 2329–2334, 2018. DOI 10.1109/IECON.2018.8592733

[20] F. Piotr, "Finite control set model predictive control for grid-connected NPC converter with LCL filter and novel resonance damping method," *in 2017 19th European Conference on Power Electronics and Applications* (EPE'17 ECCE Europe), pp. P–1. IEEE, 2017.

[21] G. V. Hollweg, P. J. D. de Oliveira Evald, E. Mattos, R. V. Tambara, and H. A. Gr¨undling, "Feasibility assessment of adaptive sliding mode controllers for grid-tied inverters with LCL filter," *Journal of Control, Automation and Electrical Systems*, vol. 33, no. 2, pp. 434–447, 2022.

[22] S. G. Parker, B. P. McGrath, and D. G. Holmes, "Regions of active damping control for LCL filters," *IEEE Transactions on Industry Applications*, vol. 50, no. 1, pp. 424–432, 2013.

[23] T. Liu, J. Liu, Z. Liu, and Z. Liu, "A study of virtual resistor-based active damping alternatives for LCL resonance in grid-connected voltage source inverters," *IEEE Transactions on Power Electronics*, vol. 35, no. 1, pp. 247–262, 2019.

[24] R. Guzman, L. G. de Vicu˜na, M. Castilla, J. Miret, and J. de la Hoz, "Variable structure control for three-phase LCL-filtered inverters using a reduced converter model," *IEEE Transactions on Industrial Electronics*, vol. 65, no. 1, pp. 5–15, 2017.

[25] K. Kumari and A. K. Jain, "Cascaded control for lcl filter based grid-tied system with reduced sensors," *IET Power Electronics*, vol. 16, no. 14, pp. 1526–1539 2022.

[26] J. Dannehl, F. W. Fuchs, and P. B. Thogersen, "PI state space current control of grid-connected PWM converters with LCL filters," *IEEE transactions on power electronics*, vol. 25, no. 9, pp. 2320–2330, 2010.

[27] X. Bao, F. Zhuo, Y. Tian, and P. Tan, "Simplified feedback linearization control of three-phase photovoltaic inverter with an lcl filter," *IEEE Transactions on Power Electronics*, vol. 28, no. 6, pp. 2739–2752, 2012.

[28] J. Kukkola and M. Hinkkanen, "Observer-based state-space current control for a three-phase grid-connected converter equipped with an lcl filter," *IEEE Transactions on Industry Applications*, vol. 50, no. 4, pp. 2700–2709, 2013.

[29] K. Hatua, A. K. Jain, D. Banerjee, and V. T. Ranganathan, "Active damping of output LC filter resonance for vector-controlled VSI-fed ac motor drives," *IEEE Transactions on Industrial Electronics*, vol. 59, no. 1, pp. 334–342, 2012. DOI 10.1109/TIE.2011.2141093

[30] J. Dannehl, M. Liserre, F. W. Fuchs, "Filter-based active damping of voltage source converters with lcl filter", *IEEE Transactions on Industrial Electronics* vol. 58, no. 8, pp. 3623–3633, 2010.

[31] O. Nelles, "*Nonlinear system identification: from classical approaches to neural networks, fuzzy models, and gaussian processes*", Springer Nature, 2020.

[32] J. Dannehl, C. Wessels, F. W. Fuchs, "Limitations of voltage-oriented pi current control of grid-connected pwm rectifiers with lcl filters", *IEEE transactions on industrial electronics* vol. 56, no. 2, pp. 380–388, February 2009

[33] Guan, Yuanpeng, et al. "The dual-current control strategy of grid-connected inverter with LCL filter." *IEEE Transactions on Power Electronics* vol. 34, no. 6, pp. 5940–5952, June 2019

[34] Dannehl, Jörg, et al. "Investigation of active damping approaches for PI-based current control of grid-connected pulse width modulation converters with LCL filters." *IEEE Transactions on Industry Applications* vol. 46, no. 4, pp. 1509-1517, July-Aug. 2010